Journal of Applied Electrochemistry (2006) 36:475–479
DOI 10.1007/s10800-005-9099-2

Anodic oxide coatings on Ti–6Al–4V produced from electrolyte containing Ca and P – Corrosion aspects

R. NARAYANAN and S.K. SESHADRI*
Department of Metallurgical and Materials Engineering, Indian Institute of Technology, Madras, Chennai 600 036, India
*(*author for correspondence, e-mail: sks@iitm.ac.in)*

Received 23 March 2005; accepted in revised form 7 November 2005

Key words: calcium, coating, oxide, phosphorus, thickness, Ti–6Al–4V

Abstract

Electrodeposited anodic oxide coatings were produced on Ti–6Al–4V substrates using aqueous electrolytes containing dissolved calcium and phosphorus. Different coatings were produced by varying the time periods. The coatings contained TiO as the major phase and contained very small quantities of calcium and phosphorus. All the coatings were less than 200 nm thick. A point defect model is obeyed by all the coatings.

1. Introduction

Titanium and its alloys are widely used as implant materials for failed hard tissues because of their excellent corrosion resistance and good compatibility with bone [1–3]. This high degree of biocompatibility is attributed to the natural formation of a protective, stable oxide layer on the surface [4]. There has been considerable interest in the use of the α-β alloy Ti–6Al–4V for orthopedic implants because of its fatigue strength and biocompatibility. Nevertheless, this alloy has certain limitations. Metal ions (Al and V) are released from the implant alloy and have been detected in tissues close to titanium implants [5]. The release of these elements, even in small amounts, may cause local irritation of the tissues surrounding the implant. Cell and tissue responses are affected not only by the chemical properties of the implant surface, but also by the surface topography or roughness of the implants [6].

To overcome these adverse effects, many surface treatment techniques like anodic oxidation [2, 7–8], sol–gel method [9], electrophoretic deposition [10] and ion implantation [11] are used. Anodic oxidation is a superior method in terms of its capacity to form rough and porous surfaces by spark discharge at high electrolytic voltage [1] and to form relatively thick and uniform coatings at ambient temperatures [2]. It can also incorporate chemical elements from the electrolyte in order to improve protective properties [8]. The presence of calcium and phosphorus in the anodic oxide films can improve the biomaterial application of titanium alloys. Anodic oxidation of titanium in electrolytes of calcium glycero-phosphate/calcium acetate [12] and sodium glycero-phosphate/calcium acetate [1] produced both calcium and phosphorus in the oxide. The anodic oxide film displayed porosity, intermediate roughness and high crystallinity. The film was very thick without any cracks and had a Ca/P ratio of 1.67 [12].

Placement of metal in solution leads to a net dissociation of metal ions, since the oxide forming reaction is more energetically favorable than a replacement reaction. An electrical double layer forms, electrons from substrate metal travel through the metal oxide and ionize dissolved oxygen at the oxide/solution interface. The resultant anions serve as electron traps, creating a potential drop and electric field across the oxide film. The oxygen then travels through the oxide under the electric field, leading to growth and coalescence of the oxide [13]. The oxide continues to form concomitant with recrystallization, suggesting an inward movement of oxygen anions along open channels of amorphous structure and also via inward movement of anions along slower diffusion paths [14]. The nature of the oxide is an important factor which controls the electrochemical properties of oxidized titanium. And its nature is decided by the oxide formation potential. More positive formation potentials result in lower concentration of vacancies (which are electron donors). This situation leads to a lower free electron concentration and hence to a larger potential drop across the film [15].

A two-layer character is generally accepted for the formation of anodic oxide layers. This is explained by simultaneous oxide growth at the phase boundaries – metal/oxide and oxide/electrolyte. This two-layer character should result in an inner phase boundary between the oxide formed due to the transport of oxygen ions

and that formed due to the transport of titanium ions. Formation mechanisms should follow solid-state reactions (phase boundary: metal/oxide) and dissolution – precipitation reactions (phase boundary: oxide/electrolyte) [16].

Anodic films are generally amorphous when they are formed galvanostatically below the electrolyte breakdown level. Growth of amorphous anodic oxide films which continues to high voltages is terminated by dielectric breakdown after which crystalline oxide is formed [17]. Oxide growth on titanium involves an amorphous-to-crystalline transition voltage as low as 10 V [18] and therefore these films are normally crystalline. During breakdown, a high density of flaws is developed in the film. But the breakdown is effectively suppressed by alloying additions of aluminum, molybdenum, silicon and tungsten, allowing growth of uniform films containing relatively few flaws at high efficiency [19]. Breakdown of passivity or the role of alloying elements like molybdenum in enhancing the resistance to passivity breakdown is expressed in terms of a point defect model using the theory of formation and mobility of cation vacancy condensates [20].

This paper describes an anodic oxidation method of synthesizing titanium oxide coatings on Ti–6Al–4V substrates from electrolytes containing calcium and phosphorus and evaluating their corrosion properties. A correlation between chemical composition and corrosion of the coatings in simulated body fluid is made in terms of cation vacancy theory.

2. Experimental procedure

The electrolyte used contained 0.30 mol l^{-1} of calcium acetate (CA) and 0.06 mol l^{-1} of β-sodium glycerophosphate (β-GP) in water. This solution had a molar ratio of (CA) to (β-GP) of 5 [21] and a pH of 8.4.

Rectangular samples of Ti–6Al–4V of size 2 cm × 3 cm were used as anode. 304 stainless steel plate was used as the cathode to complete the electrolytic cell. The coatings were obtained by applying a constant current density of 10 mA cm^{-2}. The following sequence of operations was employed: (a) mechanical polishing (b) etching in a solution containing 1 part HF, 4 parts HNO_3 and 5 parts H_2O (c) anodizing in the electrolytic solutions at 10 mA cm^{-2} for various times as mentioned in Table 1.

A Philips (Model XD-D1) microprocessor controlled X-ray diffractometer was used to identify the various phases using Cu Kα incident radiation ($\lambda = 1.5481$ Å) and XRF was used to determine the chemical composition of the coatings. Thickness measurements were made using a Gaertner ellipsometer (Model 119 XVV) containing a He–Ne laser of wavelength 632.8 nm and employing Frenel's formula.

Electrochemical polarization of the coatings was carried out using a microprocessor controlled ACM corrosion testing unit. The coating formed the working electrode and graphite the counter electrode in Simulated Body Fluid (SBF). SBF contained 8.74 g l^{-1} NaCl, 0.35 g l^{-1} $NaHCO_3$, 0.06 g l^{-1} Na_2HPO_4 and 0.06 g l^{-1} l NaH_2PO_4 [7]. Polarization was carried out in the range −700 to 4000 mV (vs. SCE) at a scan rate of 300 mV min^{-1} and corrosion currents were obtained. Electrochemical Impedance Spectroscopy (EIS) was performed in the frequency range 10^4 to 10^{-2} Hz. Chrono-amperometric measurements were done at an external applied potential of 500 mV for 2 h and the current response to this potential with time was recorded.

Table 1. Nomenclature of the coatings

Coating time	15 min	45 min	1 1/2 h	3 h	4 1/2 h	6 h	10 h	20 h	24 h
Nomenclature	A1	A2	A3	A4	A5	A6	A7	A8	A9

3. Results and discussion

The nomenclature used for the coatings is given in Table 1. All the coatings contained TiO. Though anodic oxidation deposits phosphorus in the coating, calcium and phosphorus are not detected by normal angle XRD (Figure 1) and hence XRF was used. All the coatings had 2.7–2.8 wt. % Al and 1.8–2.1 wt. % V. Table 2 gives the thickness and levels of calcium and phosphorus present. With increasing time of electrolysis, phosphorus from the electrolyte deposits in larger quantities in the coating compared to calcium. Due to their positive charge, calcium ions are repelled by the positive charge of the anodically polarized Ti–6Al–4V surface, thus reducing their extent of incorporation in the coating. However, anions such as phosphates are attracted by the anodic surface and hence are incorporated at a higher rate in the coating.

In this study a voltage of up to 30 V was applied to obtain coatings containing TiO as the major phase. However, it was also found that an increase in the applied voltage to 180 V led to oxidation of TiO to anatase and a further increase to 225 V produced a coating containing both anatase and rutile. Table 3

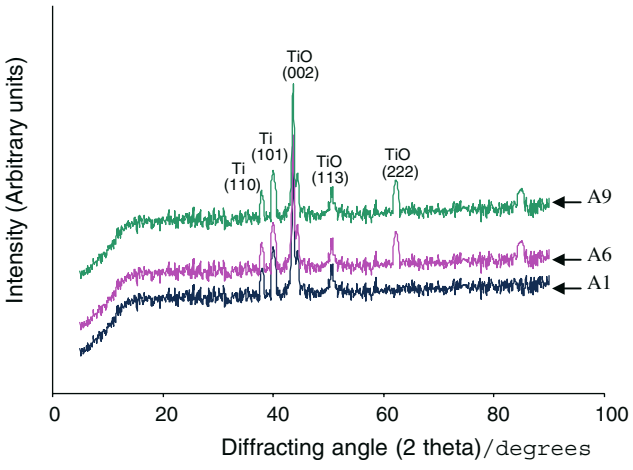

Fig. 1. XRD pattern of coatings.

Table 2. Thickness and chemical composition of coatings

Coating	Chemical composition		Thickness/nm
	Wt. % Ca	Wt. % P	
A1	0.06	0.16	90
A2	0.06	0.16	100
A3	0.06	0.16	140
A4	0.06	0.15	169
A5	0.08	0.16	152
A6	0.10	0.18	144
A7	0.17	0.22	131
A8	0.19	0.31	115
A9	0.20	0.35	110

gives the various main phases in the coating produced at different high voltages. From the Pourbaix pH-potential diagram [22] for the titanium-water system, it is observed that TiO is the predominant phase at lower potentials and TiO_2 at higher potentials, in the pH range 6–7. At 30 V, as in this study, the oxidation potential is not high enough to form the higher oxide. The measured potentials of the anodic surface (vs. SCE) also indicate that they lie in the TiO region of the pH-potential diagram for the titanium-H_2O system.

In a previous study of high voltage (of the order of 250 V and above) anodic oxidation of titanium alloys, from an electrolyte containing calcium acetate and calcium glycerophosphate, a much thicker TiO_2 coating

Table 3. Phases at various high voltages

Electrolyte composition	Phase			
	100 V	150 V	180 V	225 V
CA = 0.30 mol l^{-1}; β-Glycero phosphate = 0.06 mol l^{-1}	TiO	TiO	Anatase TiO_2	Anatase & Rutile TiO_2

having a Ca/P ratio of 1.67 was produced [12]. However, the present work involves a voltage of the order of 30 V maximum with the result that only a lower oxide, namely TiO, is formed with a Ca/P ratio less than 1, irrespective of the duration of electrolysis.

Coatings obtained have thickness in the range of 90–169 nm. If the coating time is short (45 min) the thickness is less. With increase in time of deposition (from 45 min to, say, 3 h), the oxide layer builds up leading to increased thickness. With further increase in time of electrolysis (in the case of coatings A7, A8 and A9), oxide layers detach from the substrate possibly owing to high stress levels, resulting in thicknesses lower than 130 nm. It is seen that 169 nm (as measured for A4) is the maximum thickness achieved under the present experimental conditions.

At an applied external potential of 500 mV, the current response with time up to 2 h was studied. It was found that steady-state currents produced in all the coatings

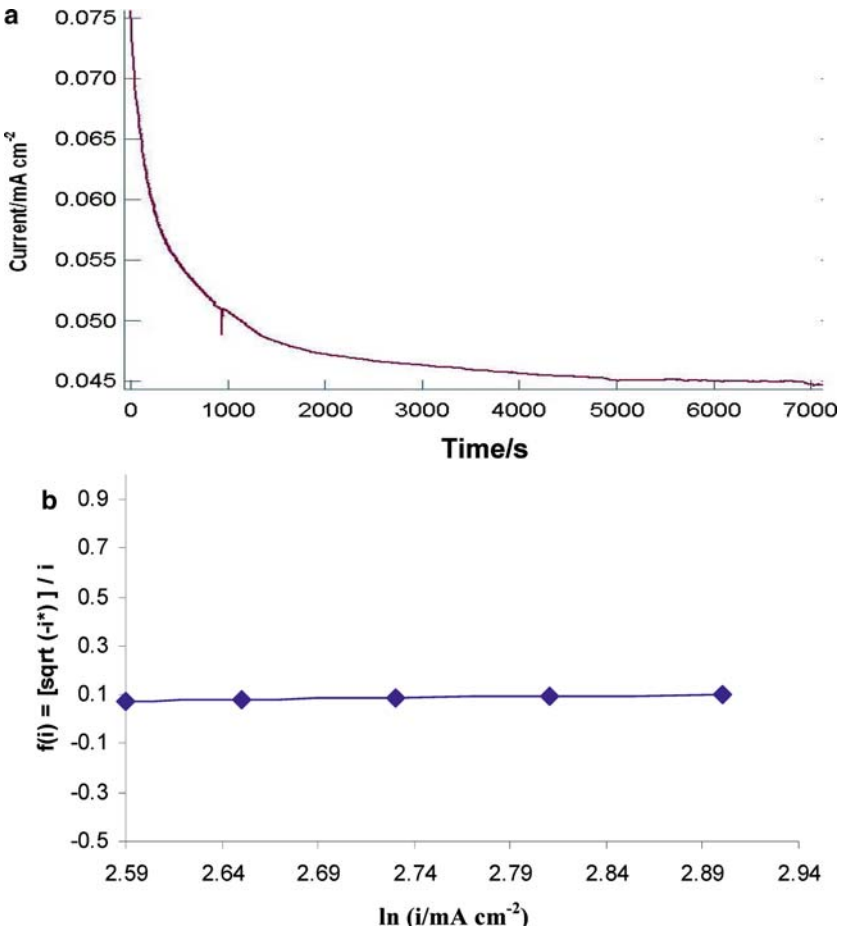

Fig. 2. A4 with 500 mV impressed potential (a) Current-transient curve (b) Plot of $-f(i)$ vs. $-\ln(i)$.

were lower than 0.1 mA cm^{-2}. A typical current response is shown for the coating A4 in Figure 2a.

It was shown by Mott [23] that the electrical field strength in a passive film (ε) can be calculated by dividing the potential drop (V) across the film by the film thickness L,

$$\varepsilon = V/L \quad (1)$$

This expression is used to explain the decrease in current with time for the growth of passive films under potentiostatic conditions (constant V). The kinetics of such a process is accounted for in terms of the High-Field Model (HFM) as

$$i = A \exp(B\varepsilon) \quad (2)$$

where i is the current density and A and B are temperature-dependent constants.

There are some discrepancies observed in HFM. According to this model a plot of activation energy vs. electric field strength should be linear and the constant A (as shown earlier) should be independent of ε. However, experimental studies on tantalum show that activation energy is not a linear function of the applied field and the factor A depends on the field strength ε [24].

Also, the HFM theory does not predict the attainment of steady-state current or film thickness. Although some modifications to this model, like dissolution at the film/solution interface, have been made to predict the attainment of steady-state current or film thickness, the predictions are neither accurate nor in agreement with the experimental results obtained for most systems which are believed to follow this model. Furthermore, HFM does not limit the field strength. For very thin films the model predicts electric field strength to be in excess of 10^7 V cm^{-1} but realistically such fields give rise to dielectric breakdown.

This model was suitably modified by Lei Zhang et al. as 'Point Defect Model' (PDM) theory [24]. According to this theory, for thin passive films like those observed in the present study, the electric field is independent of position within the film. As the steady-state film thickness varies linearly with applied voltage it was concluded that the electric field strength is independent of the applied voltage and thickness. At high fields tunneling of holes and electrons generates a counter electric field that effectively buffers the field that exists within the oxide against any process that would increase the field. The presence of (a) tunneling effect and (b) linear variation of the film thickness with applied voltage effectively eliminate the possibility of the electric field strength going beyond the breakdown strength. PDM attributes the current decrease under potentiostatic conditions to the decrease in the potential drop at the metal/film interface as the film thickens rather than to a decrease of field strength, as postulated in HFM. PDM implies that the reactions at the metal/film interface are rate-controlling. It describes the processes that occur within a barrier layer of reactions that involve the generation and annihilation of cation and anion vacancies at the metal/film and film/solution interface, respectively.

According to PDM, for a film where dissolution by the electrolyte is negligible, if i is the measured current and i^* is the differential di/dt, then a plot of

$$\frac{[-i^*]^{0.5}}{i} \quad \text{vs. ln } (i) \text{ will yield a horizontal line.}$$

From the current-transient relationships of the coatings (shown in Figure 2a), differential di/dt (also called as i^*) is calculated. A plot of $\{[-i^*]^{0.5}/i\}$ vs. ln (i) for various values of i was made and these plots for all the coatings show horizontal lines. A typical plot is shown for the coating A4 in Figure 2b. Hence it is inferred that our coatings obey the Point Defect Model (PDM). In a recent experiment on anodic oxidation of titanium in phosphoric acid it was reported that an oxide layer formed in accordance with the principles of the point defect model [25]. In explaining the behavior of Ti–6Al–4V and Ti–6Al–6Nb implants in physiological solution, the influence of niobium and vanadium on the passivity of these alloys is explained in terms of the point defect model [26].

In a similar way concepts of the point defect model can be used to explain the corrosion properties of coatings in this study. This idea is based upon cation vacancy formation and its diffusion into the lattice of the corroding system. Upon exposure to a corrosive medium cations of the system (titanium or aluminum or vanadium or calcium in the present case) dissolve at the oxide/electrolyte interface and form cation vacancies. The concentration of such cation vacancies at the metal/oxide interface will depend on (a) the relative rates of cation vacancy transport from the oxide/electrolyte interface to metal/oxide interface and (b) their annihilation at the metal/oxide interface by emission of cations from the metal into cation vacancies. If the annihilation reaction is incapable of consuming the cation vacancies arriving at the metal/oxide interface, the remaining excess vacancies will coalesce to form a cation vacancy condensate. And, if the size of this condensate exceeds a critical size, the film becomes unstable and localized breakdown takes place. This process is further aided by the presence of Cl^- ions [26].

According to the size factor the presence of elements (like phosphorus or aluminum or niobium) whose ionic radii are just higher or smaller than that of the major element (titanium in the present case) hinders corrosion.

Table 4. Ionic and covalent radii of various ions present in the coating [27]

Ions	Co-ordination number	Ionic radii/Å	Covalent radii/Å
Ti^{2+}	6	0.86	1.32
Ti^{3+}	6	0.67	1.32
Al^{3+}	6	0.54	1.43
V^{3+}	6	0.64	1.31
Ca^{2+}	6	1.0	1.74
P^{3+}		0.44	1.1
P^{5+}		0.38	1.1

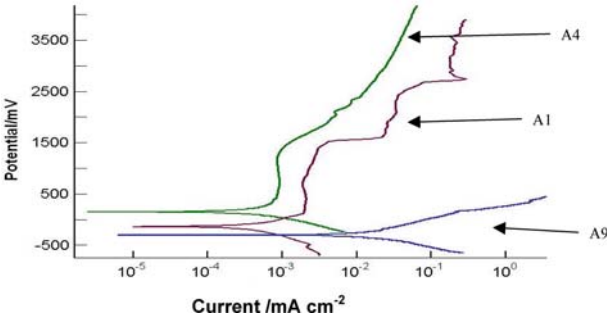

Fig. 3. Potentiodynamic polarization curves; A1 and A4 exhibit passivating type of behavior while A9 shows continuous dissolution.

A point defect occurs when the size of foreign cation (like calcium in the present case) being incorporated in the crystal lattice does not match that of the host ion. It can be inferred [27] from Table 4 that calcium ions have larger ionic radii than the host titanium ions and this situation leads to the formation of calcium cation vacancies.

The higher the concentration of calcium in the coating the greater the number of calcium ion vacancies. Further, if there is insufficient annihilation of these vacancies, localized breakdown of the oxide may occur which can lead to the attack of coatings by chloride ions of the SBF. Therefore the presence of calcium in the coating leads to corrosion. This is indicated in Table 5 where high calcium-containing coatings like A7 and A8 show more severe corrosion in the form of higher corrosion current (the potentiodynamic polarization curve in Figure 3 for A9 showing continuous dissolution in the anodic region) and lower impedance than the low calcium-containing coating like A4 (the potentiodynamic polarization curve in Figure 3 for A4 showing passivation and dissolution in the anodic region).

Calcium is an important constituent of bone. The presence of calcium on the Ti–6Al–4V implant surface promotes implant-bone biocompatibility. However, there is a difference in ionic sizes of titanium and calcium and this mismatch may result in pitting of the Ti–6Al–4V implant. This can be suitably offset by carrying out anodic oxidation to form an oxide layer of optimum thickness. In this study a coating of thickness 169 nm containing 0.06% Ca has been found to have maximum corrosion resistance. Further increase in calcium content is likely to enhance corrosion and hence could be undesirable.

4. Conclusions

Oxide coatings containing small amounts of calcium and phosphorus were produced on Ti–6Al–4V substrates by galvanostatic anodic oxidation. All the coatings contained TiO as the major phase. Coatings containing more than 0.15% calcium show increased corrosion rate. The point defect model is applicable to the coatings formed on these samples.

Table 5. Properties of anodic oxide coatings

Coating	% Ca	Potentiodynamic polarization $i_{corr}\mu$A cm^{-2}	Total impedance/ohm cm^2
A4	0.06	0.42	2.35×10^4
A6	0.10	0.65	1.99×10^4
A7	0.17	0.66	3.54×10^3
A8	0.19	2.27	2.80×10^3

References

1. H. Ishizawa and M. Ogino, *J. Biomed. Mat. Res.* **29** (1995) 65.
2. M. Shirkhanzadeh, *J. Mat. Sci.: Mat. Med.* **3** (1992) 322.
3. M. Long and H.J. Rack, *Biomaterials* **19** (1998) 1621.
4. M.A. Arenas, T.J. Tate, A. Conde and J. De Damborena, *Bri. Corr. Jl.* **35** (2000) 232.
5. G. Meachim and D.F. Williams, *J. Biomed. Mat. Res.* **7** (1973) 555.
6. D. Buser, R.K. Schenk, S. Steinemann, J.P. Fiorelini, C.H. Fox and H. Stich, *J. Biomed. Mat. Res.* **25** (1991) 889.
7. A. Cigada, M. Cabrini and P. Pedeferri, *J. Mat. Sci.: Mat. Med.* **3** (1992) 408.
8. S. Ferdjani, D. David and G. Beranger, *J All. And Comp.* **200** (1993) 191.
9. A. Montenero, G. Gnappi, F. Ferrari, M. Cesari, E. Salvioli, L. Mattogno, S. Kaciulis and M. Fini, *J. Mat. Sci.* **15** (2000) 2791.
10. Lidia Agata de Sena, Monica Calixto de Andrade, Alexandre Malta Rossi and Gloria de Almeida Soares, *J. Biomed. Mat. Res.* **60** (2002) 1.
11. M.F. Maitz, M.T. Pham, W. Matz, H. Reuther and G. Steiner, *Surf. Coat. Tech.* **158–159** (2002) 151.
12. X. Zhu, K.H. Kim and Y. Jeong, *Biomaterials* **22** (2001) 2199.
13. J.P. Jane, C.A. Orme and J.L Gilbert, *Sur. Sci.* **491** (2001) 370.
14. G.H. Gleaves, G. Dearnaley and R.A. Collins, *Th. Sol. Films* **135** (1986) L5.
15. E.N. Paleolog, A.Z. Fedotova, O.G. Derjagina and N.D. Tomashov, *J. Electrochem. Soc.* **125** (1978) 1410.
16. D. Scharnweber, R. Beutner, S. Rößler and H. Worch, *J. Mat. Sci.: Mat. Med.* **13** (2002) 1215.
17. M. Herranen and J.-O Carlsson, *Corr. Sci.* **43** (2001) 365.
18. A. Aladjem, *J. Mat. Sci.* **8**(8) (1973) 688.
19. H. Habazaki, M. Uozumi, H. Konno, K. Shimizu, P. Skeldon and G.E. Thompson, *Corr. Sci.* **45** (2003) 2063.
20. D.D. Macdonald, *J. Electrochem. Soc.* **139** (1992) 3434.
21. H. Ishizawa and M. Ogino, *J. Biomed. Mat. Res.* **29** (1995) 1071.
22. M. Pourbaix, *Atlas d'quilibre electrochimique* (Gauthier-Villars & Cie, Paris, 1963).
23. N.F. Mott, *Trans. Faraday Soc.* **43** (1947) 429.
24. L. Zhang, D.D. Macdonald, E. Sikora and J. Sikora, *J. Electrochem. Soc.* **145** (1998) 898.
25. K.S. Raja, M. Misra and K. Paramguru, *Mat. Let.* **59** (2005) 2137.
26. M. Metikoš-Huković, A. Kwokal and J. Piljac, *Biomaterials* **24** (2003) 3765.
27. Chapter 12. *in* R. David Lide (Ed.), Properties of solids in CRC Handbook of Chemistry and Physics. 82nd edition; (Boca Raton, Florida) pp 12 and 14.